Third sound on CaF_2 films of varying roughness

D. R. Luhman* and R. B. Hallock
Laboratory for Low Temperature Physics, Department of Physics, University of Massachusetts, Amherst, Massachusetts 01003, USA
(Received 31 January 2006; revised manuscript received 23 May 2006; published 17 July 2006)

The propagation of pulsed third sound on a series of CaF_2 substrates with varying roughness has been studied. The third sound speed is reported over a large range of ^{4}He film thickness including a detailed study near the onset of superfluidity. The shapes of the received third sound pulses are also reported over a large range of ^{4}He film thickness. Hysteresis is seen in the third sound speed on the roughest surfaces at low ^{4}He coverage, likely caused by capillary condensation of fluid on the surface structure. The hysteresis loops change with the roughness of the surface.

DOI: 10.1103/PhysRevB.74.014510 PACS number(s): 68.35.Ct, 68.55.Jk, 68.55.Ac, 81.15.Ef

I. INTRODUCTION

The extraordinary superfluid properties of helium at sufficiently low temperatures allow for the existence of various sound modes. One of these modes is present in very thin films of helium where the film thickness is much less than the viscous penetration depth. In this case the normal fluid component of the liquid helium film is viscously clamped to the substrate, but the superfluid component is free to move. Thus a surface wave, known as third sound, can be established in the thin film when superfluid is present. The existence of the wave is due to the motion of the superfluid. Positive thickness fluctuations are accompanied by negative temperature fluctuations.

Third sound was first observed experimentally in saturated ^{4}He films by measuring the film thickness oscillations optically on a stainless steel mirror.[1] Later a technique was developed that detected the temperature oscillation of the third sound using a superconducting transition edge detector.[2,3] The superconducting detector allowed for the detection of third sound in much thinner unsaturated films and is the technique commonly used today. This development greatly increased the types of substrates that could be used to observe third sound. Capacitive third sound measurements[4,5] and third sound resonators[6,7] allow for greater temperature flexibility and have also been used extensively in the investigations of third sound.

Initially substrates with a smooth surface, such as glass, were used in investigations of third sound.[3] More recently substrates with rough surfaces and tortuous multiply connected geometries have been studied. Third sound is studied not only for its intrinsic interest, but also as a tool to explore the superfluid transition and other wave phenomena. Many substrates have been investigated experimentally including rough metal,[8] Vycor glass,[9,10] sparsely distributed Al_2O_2 powders on glass,[11] packed,[12–14] and sintered[16] Al_2O_3 powders, alumina ceramic,[15] Nuclepore,[17,18] both etched,[19] and patterned silicon[20,21] and CaF_2 deposited on glass.[22,23]

Here we present additional data and further analysis taken in an experiment involving a series of well characterized[24] rough CaF_2 surfaces.[23] The roughness of CaF_2 films can be altered by changing the deposition thickness.[24,25] This changing roughness in turn effects the characteristics of third sound propagating across the surface, and these characteristics of third sound are what we report here. In addition there has been recent experimental[26,27] and theoretical[28] interest in the properties of the superfluid transition in helium films adsorbed to two dimensional, disordered substrates. We also report measurements of third sound near the onset of superfluidity on a range of CaF_2 film thicknesses.

II. THIRD SOUND BACKGROUND

At low temperatures, adding ^{4}He to an evacuated chamber allows for the formation of an adsorbed thin film on the surfaces inside the chamber that is in thermal equilibrium with the surrounding vapor. If the vapor pressure in the chamber, P, is sufficiently small compared to the saturated vapor pressure, P_0, adsorbed films can be atomically thin. In the experiments presented here, $P<P_0$, a condition for which adsorbed films are traditionally said to be unsaturated.

In unsaturated films, such as those used here, gravity is not relevant and the dominant attraction between a helium atom in the adsorbed film and the substrate surface is due to the van der Waals force. For an atom a distance d from a flat substrate, the force per unit mass, f, is given by

$$f = \frac{\partial \mu_v}{\partial d} = \frac{\alpha\beta(3\beta + 4d)}{d^4(d+\beta)^2}. \tag{1}$$

μ_v is the van der Waals chemical potential

$$\mu_v = -\frac{\alpha\beta}{d^3(d+\beta)}, \tag{2}$$

α is the van der Waals constant, and β is a constant associated with retardation effects.[29] The equilibrium thickness of the adsorbed film in the cell can be written as a function of P by equating the chemical potential of an atom on the surface of the film to that of an atom in the vapor. Using the chemical potential of an ideal gas at a temperature T the equation for d can be written as

$$\frac{d^4}{\beta} + d^3 = \frac{\alpha}{T\ln(P_0/P)}. \tag{3}$$

For the case of ^{4}He adsorbed on glass α=27 (layers)^{3}K and β=41.7 layers. One layer of ^{4}He is defined as 0.36 nm.

In the case where the substrate has curvature, surface tension must be taken into account. The chemical potential of an

atom on the surface then becomes $\mu=\mu_v+\mu_s$ with

$$\mu_s=\frac{\sigma}{\rho}\left(\frac{1}{R_1}+\frac{1}{R_2}\right), \tag{4}$$

where σ and ρ are the surface tension and density of bulk helium, respectively. R_1 and R_2 are the radii of curvature of the free surface of the film in two orthogonal directions.

For unsaturated helium films thicker than some critical thickness superfluidity is present, which allows for the propagation of third sound. On a smooth surface the speed of third sound is given by[30]

$$C_3^2=\frac{\langle\rho_s\rangle}{\rho}fd\left(1+\frac{TS}{L}\right)^2, \tag{5}$$

where $\langle\rho_s\rangle/\rho$ is the effective superfluid fraction in the film, S is the entropy and L is the latent heat and f is given by Eq. (1). For the temperature used here, the effective superfluid fraction in the film is customarily defined as[31]

$$\frac{\langle\rho_s\rangle}{\rho}=\frac{\rho_s}{\rho}\left(1-\frac{D}{d}\right), \tag{6}$$

where ρ_s/ρ is the bulk superfluid fraction. The quantity D has been determined empirically[31] to be $D=a+bT\rho/\rho_s$ with $a=0.5$ layers and $b=1.13$ layers/K. The quantity D can be interpreted as the part of the film that is tightly bound to the substrate and does not participate in third sound.

III. EXPERIMENTAL DETAILS

The samples used in this experiment consist of CaF_2 deposited on glass microscope slides. Before the CaF_2 deposition, strips of silver and aluminum were deposited on the glass slide to function as third sound drivers and superconducting detectors. The value of the nominal CaF_2 film coverage, t, was determined from the mass deposited as observed on a quartz crystal microbalance, measured simultaneously with the deposition on each glass substrate. The coverage, t, is reported here as a nominal film thickness presuming the bulk density of CaF_2. The film thicknesses, t, used to refer to each sample are nominal due to the nonzero porosity of the deposited CaF_2 films. The contribution to the actual CaF_2 film thickness, t_p, from the CaF_2 is t. The two quantities t and t_p are related by[24]

$$t_p=\frac{t}{1-\phi} \tag{7}$$

with the porosity $\phi\approx0.46$, independent of coverage.[24] The substrates used here had the following nominal thicknesses of CaF_2: $t=50$, 125, 220, 370, 520 nm, and plain glass (no CaF_2). The full details of sample fabrication have been presented elsewhere.[24]

Once the fabrication of the substrates was completed the samples were mounted with GE 7031 insulating varnish on copper supports in a brass sample chamber. The third sound drivers and detectors were attached to electrical leads using indium solder. The assembly was inserted into a pumped-bath ^{4}He Dewar and the system was reduced to the operating temperature.

To generate pulsed third sound a 50 μs wide square voltage pulse was applied to the silver third sound driver. The pulses were applied at a rate of 43 Hz with a typical drive energy of $\sim$100 nJ per pulse at $T=1.671$ K. The received third sound pulse was detected by monitoring the voltage across the current-biased superconducting detector. The bias current used for the detectors ranged from 10 to 100 μA. When the pulsed third sound waves arrive at the superconducting transition edge detector, the change in temperature associated with the third sound pulse changes the resistance of the detector which is recorded as a change in voltage. The signal was amplified and then sent to a digitizer. To improve the signal to noise ratio we averaged 1000 third sound pulses. The time of flight, τ, is taken from the leading edge of the averaged third sound pulse. The speed of third sound is then calculated using $C_3=l/\tau$ where l is the macroscopic distance between the driver-detector pair. For all data reported here $l=0.508$ cm. For a typical data run ^{4}He was incrementally added to the sample cell. After each addition the sample cell was allowed to thermally equilibrate and third sound pulses were then recorded on each sample involved in the particular data run. A similar procedure was used during the incremental removal of ^{4}He. The pressure of the sample cell, P, and the pressure of the Dewar bath, P_0, were also measured after each addition or removal of ^{4}He. The temperature, T, of the system was determined from the saturated vapor pressure, P_0. For all the data reported here $T=1.671\pm0.001$ K.

The third sound data presented here were taken in several different ^{4}He addition and removal runs. In a single addition or removal run third sound data were collected on all substrates where the ^{4}He film thickness on glass, d_g, spanned $0\leq d_g\leq13$ layers. d_g was calculated using Eq. (3) with $\alpha=27$ (layers) ^{3}K and $\beta=41.7$ layers for ^{4}He on glass. In a separate addition-only run data were taken on all substrates with $7.2\leq d_g\leq26.6$ layers. The results of both of these runs are reported in Sec. IV. The third sound data presented in Sec. V were only taken near the onset of superfluidity. In this case the data for each substrate were taken during a separate addition run.

After the completion of the low temperature measurements the surfaces of the substrates were imaged using atomic force microscopy (AFM). A detailed analysis of the resulting images and surface features found evidence for power-law noise.[24,32] As the thickness of the deposited film increased the typical size of the surface structures also increased in both width and height. The number of structures decreased as t increased. The actual film thickness, t_p, was measured using a profilometer giving the porosity from Eq. (7), which we found to be $\phi\approx0.46$ independent of t. See Refs. 24 and 32 for complete results and a thorough discussion of the characterization of this and another set of substrates that span a similar range of t.

IV. THIRD SOUND DATA

Figures 1 and 2 show the third sound speed and index of refraction respectively on each surface for both the addition and removal of ^{4}He as has been reported previously.[23] The

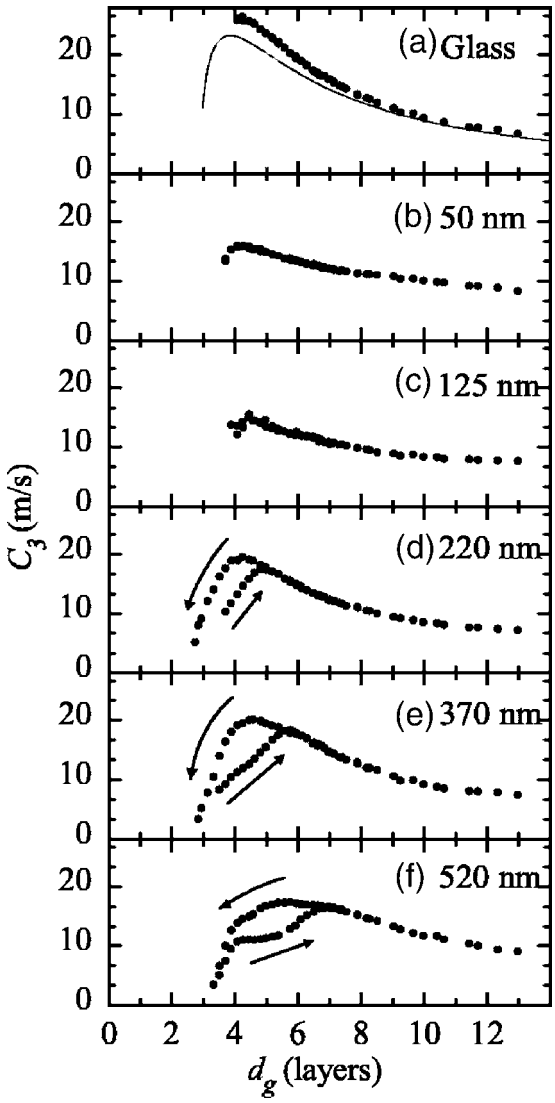

FIG. 1. Third sound speed vs d_g for all substrates at $T=1.671$ K where the number in each panel corresponds to t. The arrows indicate the addition and removal of ^{4}He. The solid line in panel (a) is obtained from Eq. (5) using the parameters for glass stated in the text.

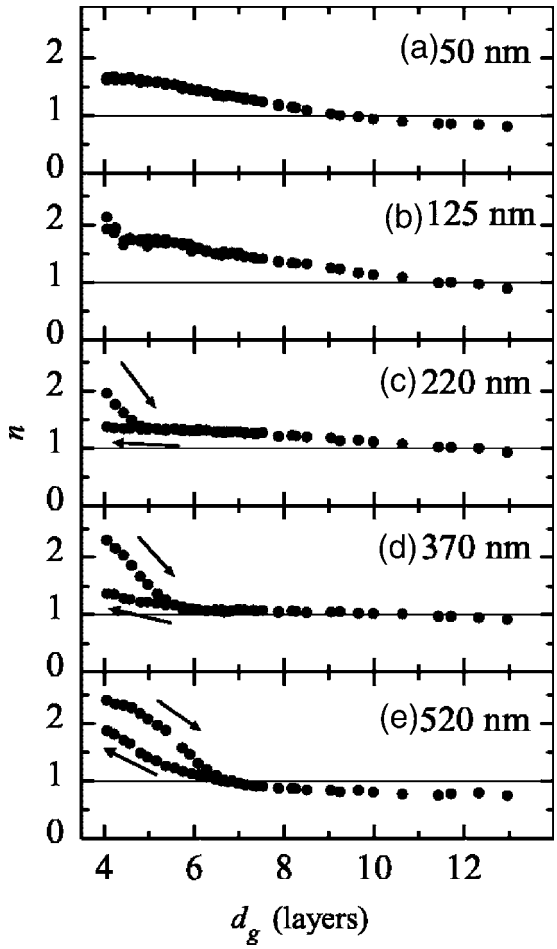

FIG. 2. The index of refraction, n, versus d_g for the CaF_2 surfaces for $T=1.671$ K. The arrows indicate the addition and removal of ^{4}He and the horizontal solid lines denote $n=1$.

index of refraction, n, for the CaF_2 surfaces is defined as $n=C_g/C_{CaF_2}$ where $C_g(C_{CaF_2})$ is the speed of third sound on glass (CaF_2). The glass substrate shows no hysteresis and behaves similar to what is expected from Eq. (5). This is shown by the solid line in Fig. 1(a) calculated from Eq. (5) using the above stated parameters. For the $t=50$ nm and 125 nm substrates, no hysteresis is seen but the speed of third sound is less than on glass ($n>1$) for small values of d_g. For $t\geq 220$ nm hysteresis is seen for small values of d_g. The origin of the hysteresis is likely the capillary condensation of fluid into the surface structure of the CaF_2. As t increases the loops shift to higher d_g, indicating that the size of the surface structure is also increasing in agreement with the AFM results.[24] The hysteresis due to the capillary condensation is broad, presumably due to the distribution of pore sizes. The loops in Fig. 2 do not close for small values of d_g because third sound is not present on glass for $d_g<4.05$ layers, therefore n is not defined in this region. Third sound is found to propagate at lower values of d_g on the rough CaF_2 than on glass. This is most likely due to the additional adsorption of helium on the surface[22,26] and is discussed in more detail below. This hysteretic behavior is robust and reproducible.

The shape of the hysteresis loops is due to a variety of factors. The tortuous propagation path, the nonuniform film thickness and the resultant effects on $\langle\rho_s\rangle/\rho$ all contribute to the observed value of C_{CaF_2}. The CaF_2 surfaces are not smooth and surface tension may play an important role in f. The size of the nominal surface structure of the CaF_2 is on the order of 10 nm.[24] As a rough estimate, of μ_s [see Eq. (4)] we use the typical surface structure size for $R_1=R_2\sim 10$ nm and find that μ_s is significant when compared to μ_v for the studied ^{4}He coverages. Therefore the total chemical potential used to calculate f will be a sum of μ_v and μ_s for these surfaces. Due to the tortured and random nature of our surfaces it is not feasible to know explicitly how the radius of curvature of the free surface and the local film thickness change as a function of position on the substrate. Therefore it is impossible to model our rough surfaces with the direct application of Eq. (5).

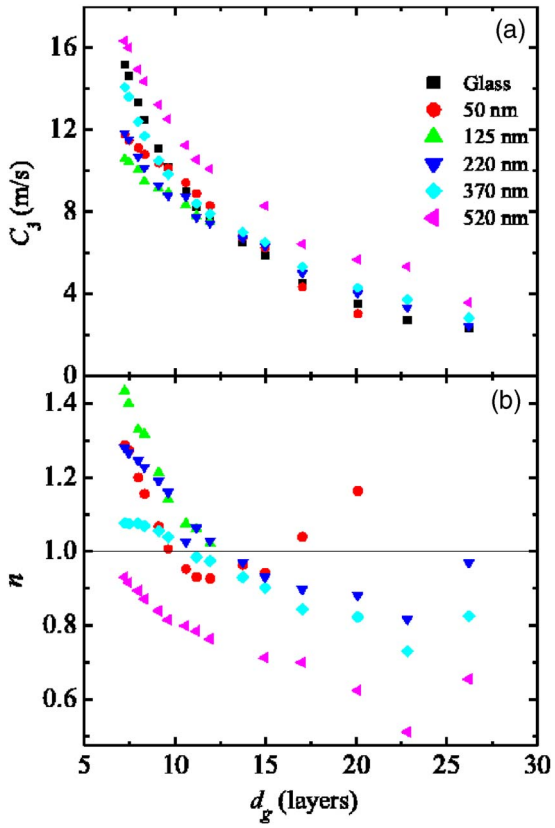

FIG. 3. (Color online) (a) Speed of the observed sound mode and (b) the corresponding n versus d_g for all surfaces in the regime of large d_g (where hysteresis is absent) as ^{4}He is incrementally added to the sample cell. In this regime the received third sound signals were small. Due to the relatively low sensitivity of the $t=125$ nm detector, data could not be collected on that substrate out to the thickest coverages. The solid line in (b) represents $n=1$.

Studies[12] of sound modes in packed Al_2O_3 powders have investigated the contribution of surface tension to the speed of the observed sound in conjunction with measuring the amount of adsorbed ^{4}He. The data in Fig. 1 for the $t=520$ nm substrate are reminiscent of the data sets in Rosenbaum *et al.*,[12] including the feature near $d_g=4$ layers. This feature or "knee" was interpreted in Ref. 12 as the onset of capillary condensation, and we expect a similar situation for our substrates. However, there is an important difference in the data beyond the knee. The substrate of Rosenbaum *et al.* was a three dimensional annulus of packed powder and as all the pores filled with helium the speed of the observed sound became very large as the system crossed over to fourth sound. In our data, C_{CaF_2} increases beyond the knee, reaches a peak and then begins to decrease. Since we are dealing primarily with surface roughness, the film should not have a major contribution from fourth sound, consistent with the observed decrease in C_{CaF_2}. However, as d_g gets very large, the speed of the sound mode on the rough CaF_2 is greater than that on the smooth glass ($n<1$) as seen in Figs. 3 and 4. In this region this may be due to coupling to fourth sound in the porosity beneath the surface. As d_g becomes very large the speed of third sound becomes less dependent on the roughness of the surface as is readily apparent in Fig. 4. This

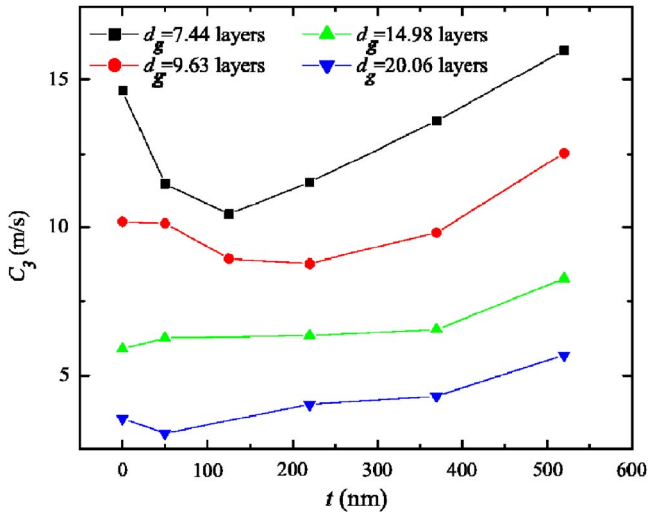

FIG. 4. (Color online) Third sound speed as a function of t for several values of d_g in the thick film regime. Data points have been connected by line segments as a guide to the eye. The points at $t=0$ represent the glass substrate.

could be related to additional contributions to the observed sound, such as surface tension, on the rough surfaces being washed out in the extreme thick film limit.

V. SUPERFLUID ONSET

The superfluid transition for thin helium films on flat surfaces has been successfully described by Kosterlitz-Thouless[33] (KT) theory and its modifications to include finite frequencies.[34,35] One of the most interesting predictions resulting from KT theory is the discontinuous jump in areal superfluid density, σ_s, at the transition temperature T_c.[36] The jump is given by the universal relation

$$\frac{\sigma_s}{T_c} = \frac{2m^2k_B}{\pi\hbar^2} = 3.49 \times 10^{-8}\ \text{kg/m}^2\,\text{K}, \tag{8}$$

where m is the mass of one helium atom. The actual observed jump is slightly rounded due to finite frequencies and flow velocity. If we define the areal superfluid density as $\sigma_s=\langle\rho_s\rangle d_g$, we can use the third sound data and Eq. (5) to study the superfluid transition on glass as was first pointed out by Rudnick.[37] Near the transition the effects due to retardation are minimal ($d_g/\beta \ll 1$) and we can use $f=3\alpha/d_g^4$ as the van der Waals restoring force and $d_g^3=\alpha/[T\ln(P_0/P)]$ to calculate d_g. Using this simplified expression for f and the definition of σ_s, Eq. (5) can be written as

$$\frac{\sigma_s}{T} = \frac{C_g^2 d_g^4 \rho}{3\alpha T(1+TS/L)^2} \tag{9}$$

for glass. We have replaced T_c with our operating temperature T. Figure 5 shows data from a subsequent more detailed run in the vicinity of the KT transition on glass. C_g and σ_s/T calculated from Eq. (9) are shown in the figure as a function of d_g from data taken during the incremental addition of ^{4}He.

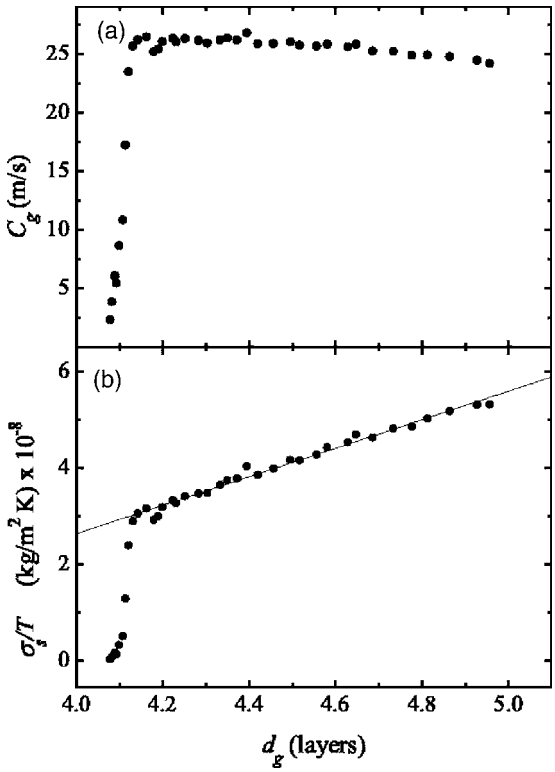

FIG. 5. (a) C_g and (b)σ_s/T versus d_g in the KT transition region for glass. The solid line in the lower panel is a linear fit to the data.

Once third sound becomes visible, the rise in C_g and σ_s is quite dramatic. Beyond the sharp increase in σ_s the σ_s/T data become linear in d_g as expected from Eq. (6). At the knee, $\sigma_s/T=3.15\times10^{-8}$ kg/m^2 K modestly close to the predicted jump in Eq. (8) of 3.49×10^{-8} kg/m^2 K. The intercept of the horizontal axis of a linear fit to σ_s/T beyond the knee yields a value of $D=3.1\pm0.1$ layers, near the value $D=2.9$ layers given by the empirical rule noted previously.

The abrupt onset of superfluidity has been experimentally observed to decrease with increasing thickness of CaF_2 in quartz oscillator studies.[26,27] Beyond $t\approx100$ nm little or no signature was observed signifying the onset of superfluidity. The largest value of t investigated in this way was $t=300$ nm.[22] Figure 6 shows σ_s/T calculated from Eq. (9) for the CaF_2 samples. These plots cannot be interpreted quantitatively because Eq. (5) does not account for surface tension contributions and the vertical axes are calculated using d_g. The actual film thickness is not uniform, and the amount ^{4}He adsorbed onto the surfaces is not known explicitly, but it is estimated as being nearly an order of magnitude greater than on glass.[22] In addition, no compensation was made for the index of refraction not being equal to unity on these samples. Together these factors preclude any additional analysis. Nonetheless it is interesting to compare the shapes of the curves to that for glass. For $t=50$ nm the initial increase in σ_s/T is still sharp and beyond the increase the data are linear. The $t=125$ nm data are unusual with a small step after third sound is first observed followed by a gently sloped region and then a larger step. Beyond $t=125$ nm, the initial slope of σ_s/T is not steep. Rather the increasing curves are relatively featureless. Qualitatively these results are in agreement with the quartz oscillator studies.

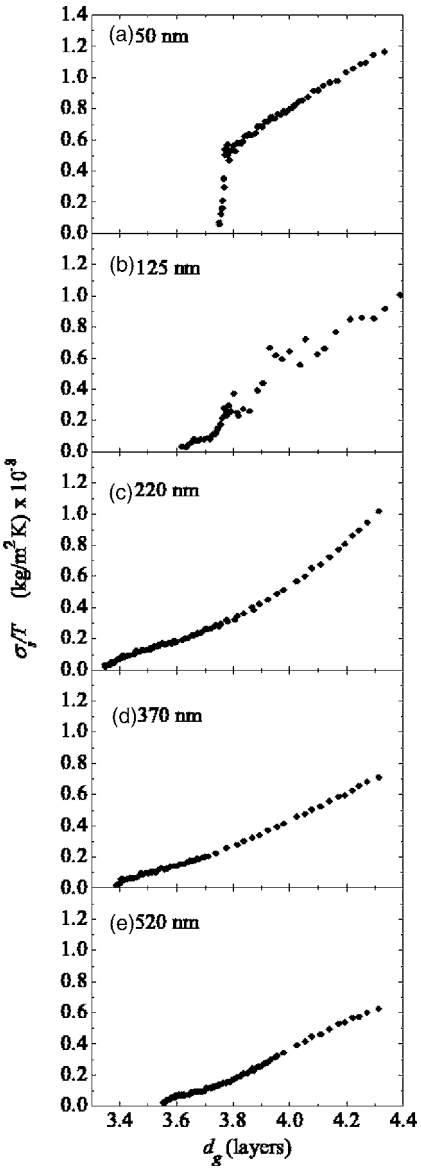

FIG. 6. σ_s/T versus d_g in the KT transition region for the CaF_2 samples. The vertical axis on each panel is similar.

From Figs. 5 and 6 the differences in the value of d_g where third sound is first observed, d_s, for different values of t is quite apparent. Figure 7 plots d_s versus t, where $t=0$ nm corresponds to the glass substrate. d_s is the thickness observed on glass when third sound is observed on a CaF_2 substrate. Glass has the highest value of d_s, as might be expected since it also likely has the least amount of absorbed helium. There is a dip in the data at $t=220$ nm, which may give us insight into the structure of the helium film in this region of d_g. For the $t=50$ and 125 nm samples capillary condensation, if it is present, occurs before the onset of third sound as is apparent in Fig. 1, while for the $t=520$ nm sample the onset of capillary condensation appears to occur after third sound is present. For $t<300$ nm the amount of ^{4}He adsorbed at a particular value of d_g increases as t increases.[22,26] Thus for these samples where capillary condensation occurs before the onset of third sound we expect a

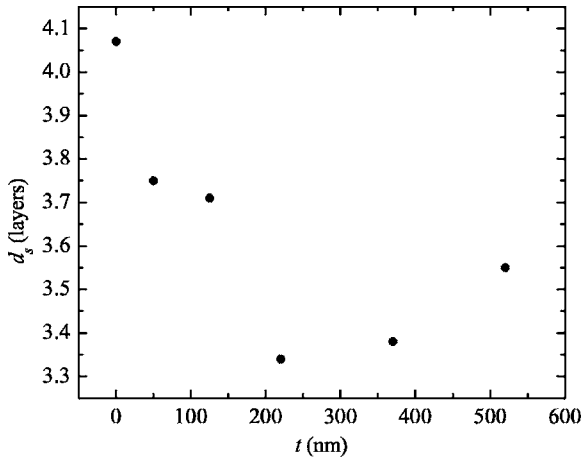

FIG. 7. d_s versus t for all the substrates. The point at $t=0$ nm represents the glass substrate.

decreasing trend in d_s as t increases since the amount of adsorbed fluid also increases. For those samples whose typical pore size is large enough that capillary condensation occurs after third sound is present, such as for the $t=520$ nm sample, we expect d_s to be larger than for those samples where capillary condensation occurs before the onset of third sound. This is because capillary condensation has not yet occurred and there is less fluid expected to be adsorbed on the surface. In the limit of very large pores, the value of d_s would likely coincide with that of glass. The crossover from one type of behavior to the other will occur when the onset of third sound and capillary condensation coincide. This crossover will occur gradually for our system because the pores are described by a distribution of sizes rather than by a single size and the curvature of the surfaces will also cause changes in film thickness and the amount of ^{4}He adsorbed. From Fig. 7, this is the type of behavior we observe and the crossover appears near $t=220$ nm, which is consistent with the amount of adsorption of ^{4}He also increasing as t increases for $t<300$ nm. This hypothesis is also consistent with the earlier stated interpretation of the knee being the onset of capillary condensation in the $t=520$ nm data in Fig. 1. Adsorption isotherms have not been measured for $t>300$ nm.

VI. THIRD SOUND PULSE SHAPE EVOLUTION

In Fig. 8 we have plotted the received third sound pulses

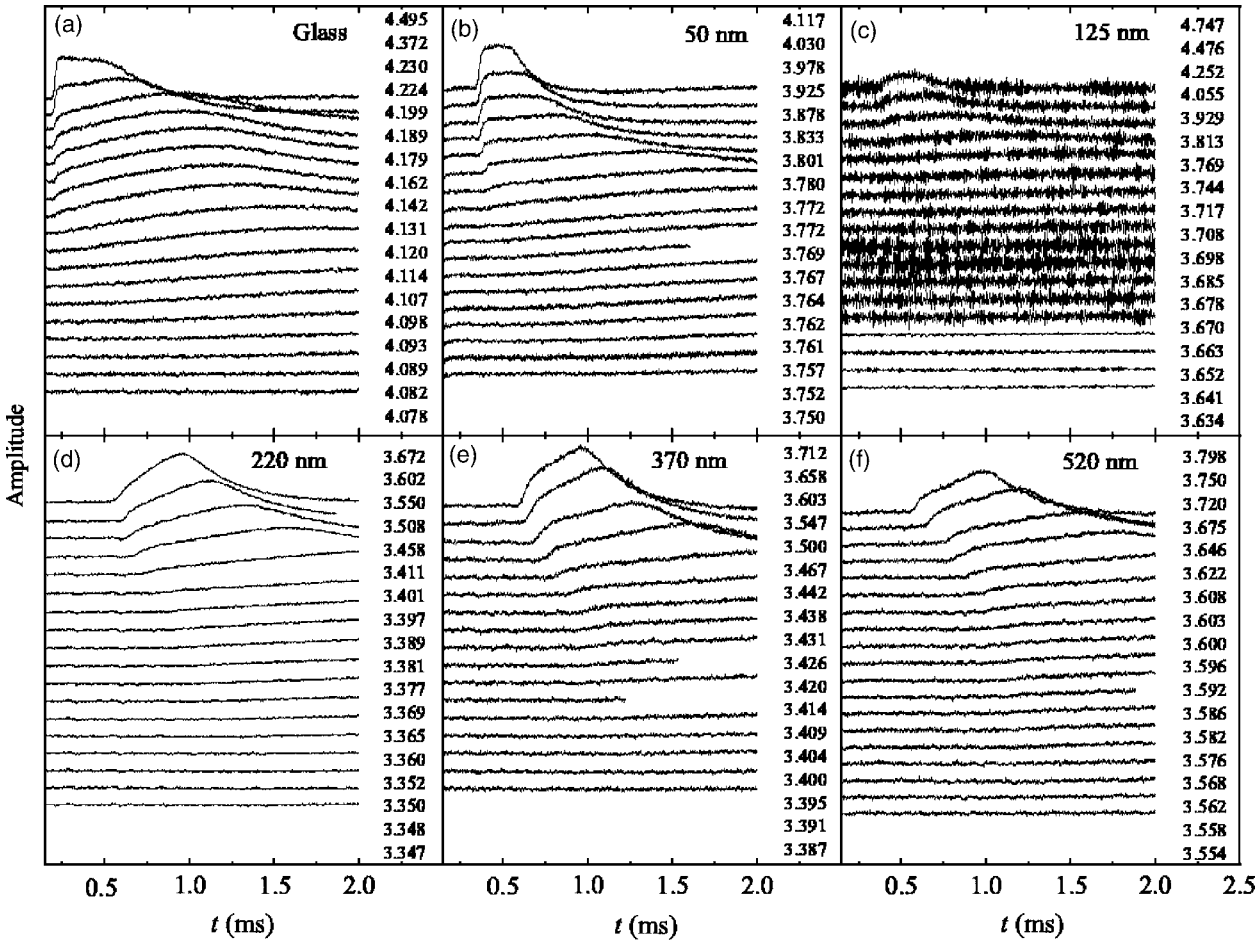

FIG. 8. Evolution of the received third sound pulses on all samples near the KT transition. In all cases the third sound drive was a 50 μs wide square pulse. The row of numbers in each panel correspond to d_g in layers for that set of pulses. The detector for the 125 nm sample was less sensitive than the detectors on the other samples, thus the signal to noise ratio is lower for the case of 125 nm. The data in each section of the plot are offset vertically for clarity and the vertical axis is arbitrary for each panel.

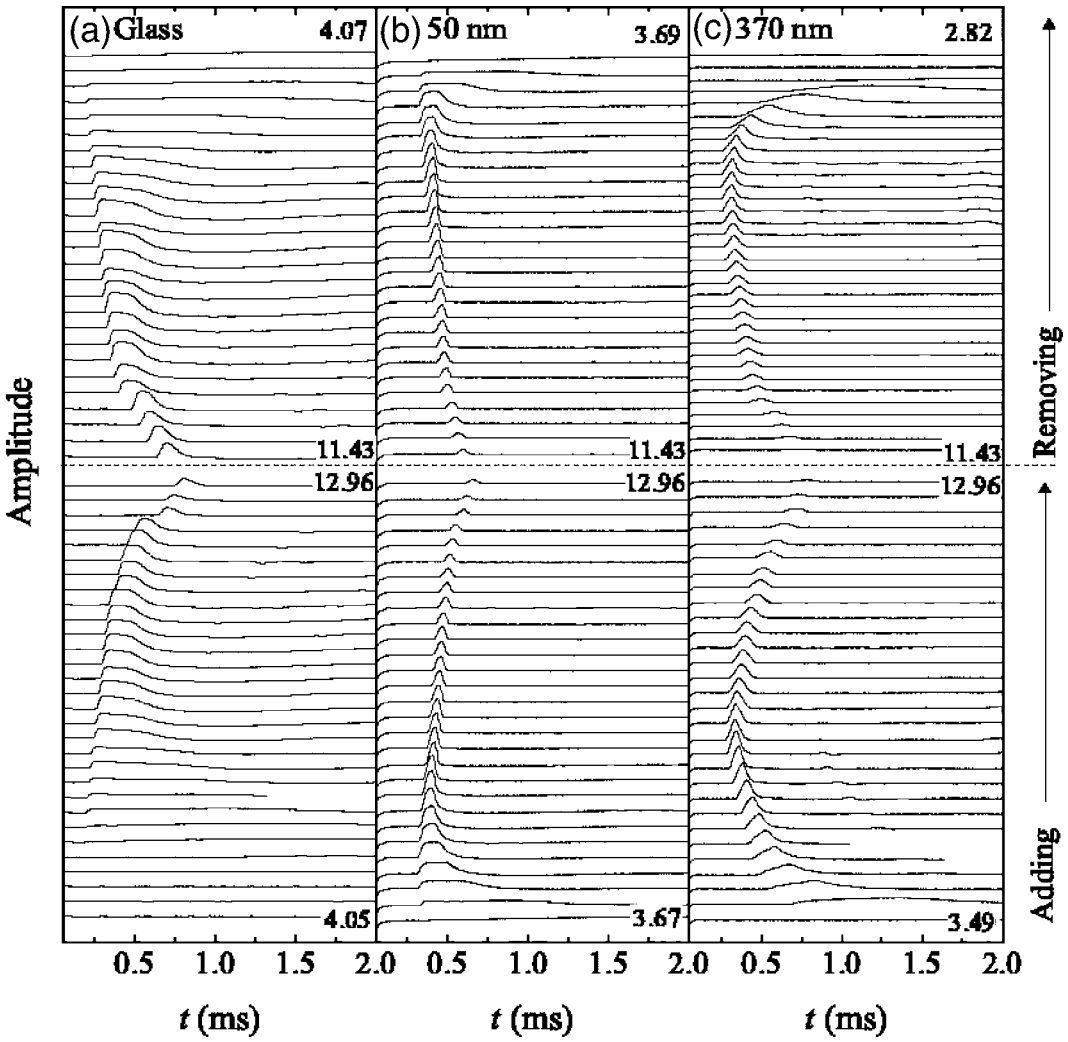

FIG. 9. Evolution of the pulses on the plain glass substrate, the $t=50$ nm substrate, and the $t=370$ nm substrate for the adding and removing data shown in Fig. 1. The third sound pulses are plotted in waterfall format with d_g increasing from the bottom trace of the figure to the dashed line. Above the dashed line the pulses are shown with decreasing d_g. The numbers on the various sections of the data indicate values of d_g. The small wiggles visible to the right of several of the main pulses are reflections from adjacent third sound drivers. The units on the vertical axis are arbitrary for each panel.

near the observed onset of superfluidity.[38] The data are plotted in waterfall format with d_g increasing from the bottom to the top as shown by the vertical row of numbers in each panel. In all cases the initial third sound signal was quite broad and detected by a subtle change in the slope of the signal. As d_g was increased the pulses became less broad and more well defined. Of the signals that are more defined, a slight difference can be noted in the shape of the signals. The signals for rougher substrates, shown in panels (d)–(f), appear peaked with two distinct regions of increase. The signals for the less rough substrates, shown in panels (a)–(c), on the other hand, are flatter. The exact origin of this behavior is not clear. However, on the substrates with two regions of increase the first increasing region persists for approximately 50 μs which is also the width of the input drive pulse. As d_g increases further these pulses become more symmetrical and the 50 μs region of rapid increase is no longer present, as shown in Fig. 9. One possibility is that CaF_2 itself is absorbing a portion of the input energy which continues to contribute to the amplitude of the wave after the drive pulse has ended.

The shape of the pulses for the larger d_g traces shown in Fig. 9 also indicate that the third sound is in some cases likely overdriven and perhaps even saturated.[39] The same drive power was used on all samples over an entire run. Due to the increase in helium adsorption on the rougher samples, more drive voltage was needed to produce third sound on those samples at thicker coverages of ^{4}He. We should note that overdriving a third sound pulse does not significantly alter the time of flight of the leading edge of the observed pulse as is indicated by the data in Ref. 39 and thus does not affect the result of our measurements of the speed of the observed third sound.

VII. CONCLUSIONS

We report a series of observations involving the characteristics of third sound on thermally deposited CaF_2 spanning

a range of thicknesses and thus roughnesses. We again report[23] the hysteric behavior of the third sound speed and index of refraction on substrates. In addition we show third sound data for large ^{4}He coverages and observe that the speed of the propagating sound mode is faster on the rougher samples than on glass. We have also investigated the thin film behavior of third sound near the observed KT transition. For glass we obtain modest agreement with predictions for the jump in the superfluid density. While on the CaF_2 substrates with $t > 125$ nm the shape of the σ_s/T curves is smooth and relatively featureless. The value of d_g where third sound is first observed, d_s, changes as t increases and has a minimum near $t=220$ nm. We have also shown the evolution of the shape of the third sound pulse near the onset of observed superfluidity for all substrates.[40] Further interpretations of this type of data will require a measurement of the amount of helium adsorbed to the surface, which could be done capacitively.

ACKNOWLEDGMENTS

Figures 1 and 2 are adapted from an original figure [Fig. 1 in D. R. Luhman and R. B. Hallock, J. Low Temp. Phys. **138**, 319 (2005)] with the kind permission of Springer Science and Business Media. This work was supported by the National Science Foundation under Grant Nos. DMR-0138009 and DMR-0213695 (MRSEC) and also by research trust funds administered at the University of Massachusetts Amherst. We have benefited from the facilities maintained by the MRSEC.

*Current address: Dept. of Electrical Engr. Princeton Univ., Princeton, NJ, 08544.

[1] C. W. F. Everitt, K. R. Atkins, and A. Denenstein, Phys. Rev. Lett. **8**, 161 (1962); Phys. Rev. **136**, A1494 (1964).
[2] I. Rudnick, R. S. Kagiwida, J. C. Fraser, and E. Guyon, Phys. Rev. Lett. **20**, 430 (1968).
[3] I. Rudnick and J. C. Fraser, J. Low Temp. Phys. **3**, 225 (1970).
[4] J. S. Brooks, F. M. Ellis, and R. B. Hallock, Phys. Rev. Lett. **40**, 240 (1978).
[5] A. M. R. Schechter, R. W. Simmonds, R. E. Packard, and J. C. Davis, Nature (London) **394**, 594 (1998).
[6] F. M. Ellis and R. B. Hallock, Rev. Sci. Instrum. **54**, 751 (1983).
[7] F. M. Ellis and L. Li, Phys. Rev. Lett. **71**, 1577 (1993).
[8] R. K. Galkiewicz, K. L. Telschow, and R. B. Hallock, J. Low Temp. Phys. **26**, 147 (1977).
[9] J. E. Berthold, D. J. Bishop, and J. D. Reppy, Phys. Rev. Lett. **39**, 348 (1977).
[10] D. J. Bishop, J. E. Berthold, J. M. Parpia, and J. D. Reppy, Phys. Rev. B **24**, 5047 (1981).
[11] D. T. Smith, M. Liebl, M. D. Bummer, and R. B. Hallock, in *Low Temperature Physics LT-17, Contributed Papers*, edited by V. Eckern *et al.* (North-Holland, Amsterdam, 1984), p. 57.
[12] R. Rosenbaum, G. A. Williams, D. Heckerman, J. Marcus, D. Scholler, J. Maynard, and I. Rudnick, J. Low Temp. Phys. **37**, 663 (1979).
[13] V. Kotsubo and G. A. Williams, Phys. Rev. B **28**, 440 (1983); Phys. Rev. Lett. **53**, 691 (1984); Phys. Rev. B **33**, 6106 (1986).
[14] M. Z. Shoushtari and K. L. Telschow, Phys. Rev. B **26**, 4917 (1982).
[15] H. Cho and G. A. Williams, Phys. Rev. B **64**, 144503 (2001).
[16] M. Bernard and G. A. Williams, Phys. Rev. Lett. **67**, 2585 (1991).
[17] J. M. Valles, Jr., D. T. Smith, and R. B. Hallock, Phys. Rev. Lett. **54**, 1528 (1985).
[18] D. T. Smith, K. M. Godshalk, and R. B. Hallock, Phys. Rev. B **36**, 202 (1987).
[19] D. T. Smith and R. B. Hallock, Phys. Rev. B **34**, 226 (1986).
[20] D. T. Smith, C. P. Lorenson, R. B. Hallock, K. R. McCall, and R. A. Guyer, Phys. Rev. Lett. **61**, 1286 (1988).
[21] D. T. Smith, C. P. Lorenson, and R. B. Hallock, Phys. Rev. B **40**, 6634 (1989); **40**, 6648 (1989).
[22] J. C. Herrmann and R. B. Hallock, Phys. Rev. B **68**, 224510 (2003).
[23] D. Luhman and R. B. Hallock, Bull. Am. Phys. Soc. **49**, 166 (2004); J. Low Temp. Phys. **138**, 319 (2005).
[24] D. R. Luhman and R. B. Hallock, Phys. Rev. E **70**, 051606 (2004).
[25] F. Varnier, N. Mayani, and G. Rasigni, Appl. Opt. **28**, 127 (1989).
[26] D. R. Luhman and R. B. Hallock, Phys. Rev. Lett. **93**, 086106 (2004).
[27] R. J. Lazarowich and P. Taborek, to be published.
[28] K. G. Balabanyan and N. Prokofev, to be published.
[29] See, for example, S. Putterman, *Superfluid Hydrodynamics* (North-Holland, Amsterdam, 1974).
[30] D. Bergman, Phys. Rev. **188**, 370 (1969); D. J. Bergman, Phys. Rev. A **3**, 2058 (1971).
[31] J. H. Scholtz, E. O. McLean, and I. Rudnick, Phys. Rev. Lett. **32**, 147 (1974); J. H. Scholtz, E. O. McLean, and I. Rudnick, *ibid.* **32**, 569(E) (1974).
[32] D. R. Luhman and R. B. Hallock, Phys. Rev. Lett. **92**, 256102 (2004).
[33] J. M. Kosterlitz and D. J. Thouless, J. Phys. C **6**, 1181 (1973).
[34] V. Ambegaokar, B. I. Halperin, D. R. Nelson, and E. D. Siggia, Phys. Rev. B **21**, 1806 (1980).
[35] B. A. Huberman, R. J. Myerson, and S. Doniach, Phys. Rev. Lett. **40**, 780 (1978).
[36] D. R. Nelson and J. M. Kosterlitz, Phys. Rev. Lett. **39**, 1201 (1977).
[37] I. Rudnick, Phys. Rev. Lett. **40**, 1454 (1978).
[38] For the smallest values of d_g data were collected for 3000 μs to ensure τ could be measured. These traces were truncated to 2000 μs for clarity in Figs. 8 and 9 without the loss of relevant information. Due to a computer problem, several of the signals in Figs. 8 and 9 do not show data to 2000 μs.
[39] S. Wang, K. S. Ketola, P. Lemaire, and R. B. Hallock, J. Low Temp. Phys. **119**, 645 (2000).
[40] For the case of the glass substrate, the pulse shape evolution as a function of d_g seen here is in general agreement with previous work in this laboratory; J. Maps and R.B. Hallock, 1980 (unpublished).